

Memory effects in a turbulent plane wake

Y. Zhou, R. A. Antonia

112

Abstract Memory effects in turbulent plane wakes have been investigated for various wake generators (circular, triangular and square cylinders and a screen of 50% solidity) using orthogonal arrays of X-wires, eight in the (x, y) plane and eight in the (x, z) plane. In the far-wake region, discernible differences are observed for different generators, in the measured Reynolds stresses, spectra of v and approximations to the rms spanwise and lateral vorticities. These differences, which reflect variations in various aspects of the organised large-scale structures, are quantified through the contributions these structures make to the Reynolds stresses. The difference between the screen and the solid body wakes is especially pronounced.

1

Introduction

It is now well established that turbulence does not entirely “forget” its origins – and the idea of a self-preserving state implying asymptotic independence on initial conditions is not strictly valid. One would expect memory effects to be more important in free shear flows such as jets and wakes than in wall flows where the presence of the wall tends to act as a memory “eraser”.

Indeed, there is a significant amount of evidence which points to the persistence of initial conditions in the self-preserving regions of plane and axisymmetric wakes. Bevilaqua and Lykoudis (1978) compared the wake of a sphere with that of a porous disk which had the same drag and Reynolds number, based on free stream velocity and diameter. They observed that there were differences in the self-preserving regions of these flows. For example, the turbulence intensity (normalised by the maximum velocity defect U_1) was greater in the wake of the sphere than in that of the disk. Bevilaqua and Lykoudis proposed a possible hierarchy of self-preserving states, i.e. order one when the mean velocity reaches self-preservation, order two when, in addition to the mean velocity, Reynolds stresses become self-preserving, and so

on through higher-order moments. Wygnanski et al. (1986) investigated turbulent plane wakes ($x/\theta = 100 \sim 2000$, where x is the streamwise co-ordinate and θ is the momentum thickness) behind various generators, with approximately the same drag coefficient. Normalised profiles of the streamwise mean velocity \bar{U} were virtually identical but the shapes of the normalised longitudinal turbulence intensity $\overline{u^2}$ and Reynolds shear stress \overline{uv} seemed to depend on initial conditions, even though they conformed, for a particular flow and set of initial conditions, with self-preservation. The studies by Bonnet et al. (1985), Louchez et al. (1987) and Cimbala et al. (1988) have confirmed that the detailed behaviour of a turbulent far-wake can depend significantly on initial conditions.

George (1989) carried out a self-preservation analysis for jets and wakes with a view to provide a suitable framework for the possible relationship between self-preservation, initial conditions and coherent structures. His analysis indicated that, when normalised by U_1 and the half-width L , Reynolds shear stress profiles in a particular flow, e.g. a plane wake, should have similar shapes but different amplitudes. In the case of the Reynolds normal stresses, both their shape and amplitude may depend on initial conditions. These results are consistent with the observations of Wygnanski et al. (1986).

It has been argued (e.g. Bevilaqua and Lykoudis 1978; George 1989) that there is a link between self-preservation and large-scale vortical structures. The persistence of the effect of initial conditions in the self-preserving region seems to imply that the characteristics of these structures may depend on initial conditions. Such a dependence is expected in the near and intermediate regions of the wake and the experimental evidence (Kiya and Matsumura 1985a, b; Matsumura et al. 1991) has indeed confirmed the sensitivity of organised aspects of the motion to different wake generators that have been used. For example, the data presented by Kiya and Matsumura (1985a, b) indicate some differences in topology between a circular cylinder wake and the wake of a flat plate placed normal to the flow. This type of documentation is not available for the far-wake. The main aim of this paper is to provide such information and relate it to the corresponding data in the near-wake. The large-scale vortical motion in the far-wakes produced by different generators (circular, triangular, square cylinders and a screen of 50% solidity) is compared with that obtained in the near-wakes. The comparison is both qualitative (sectional streamlines delineate the overall features of the large scale vortices) and quantitative (estimates of the strength of the vortices are given as are estimates of the contribution the vortices make to the Reynolds stresses).

Received: 29 August 1994/Accepted: 8 May 1995

Y. Zhou, R. A. Antonia
Department of Mechanical Engineering, University of Newcastle,
N.S.W. Newcastle, 2308, Australia

Correspondence to: R. A. Antonia

The support of the Australian Research Council is gratefully acknowledged

Experimental conditions

Experiments were carried out in an open return low turbulence wind tunnel with a 2.4 m long working section (0.35 m × 0.35 m). The bottom wall was tilted to achieve a zero streamwise pressure gradient. Each generator (details of the various configurations are given in Fig. 1 and Table 1) was installed in the mid-plane and spanned the full width of the working section. Measurements were made at distances ranging from 24 to 830 θ downstream of the wake generator, where θ is the momentum thickness (constant for a given generator, see Table 1). Over this range, U_1 decreased from about 0.3 U_∞ to 0.05 U_∞ (Table 1). The free stream velocity U_∞ was 6.7 m/s in all experiments.

Generators of the same characteristic dimension h ($= 12.5$ mm) were used for the near-wake investigation, the measurements being carried out at the same value of x/h

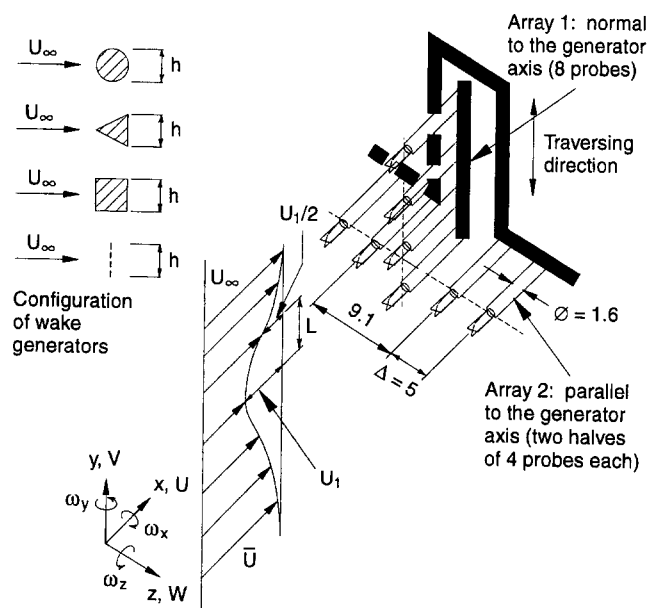


Fig. 1. Experimental arrangement

Table 1. Summary of flow parameters for various wake generators

Wake generator	h (mm)	θ (mm)	x/θ	x/h	L (mm)	Re_h	Re_θ	U_1/U_∞
Circular cylinder	2.65	1.3	780	380	12.5	1200	560	0.05
	2.65	1.3	570	280	12.0	1200	560	0.06
	6.35	3.0	580	280	25.0	2800	1300	0.06
	12.50	5.9	42	20	14.0	5600	2600	0.20
Triangular cylinder	5.30	3.2	550	330	25.5	2400	1400	0.07
	5.30	3.2	240	145	15.4	2400	1400	0.10
	12.50	7.5	33	20	18.0	5600	3300	0.22
Square cylinder	4.70	4.3	410	375	30.5	2100	1900	0.06
	4.70	4.3	180	165	19.6	2100	1900	0.10
	12.50	10.6	24	20	19.0	5600	4700	0.22
Screen	8.00	2.1	830	220	15.5	3600	900	0.06
	12.50	4.1	300	98	16.1	5600	1800	0.12
	12.50	4.1	61	20	10.0	5600	1800	0.33

($= 20$). The relatively large value of h was required primarily in order to use the same orthogonal X-wire arrays (described below) as for the far-wake measurements. In the latter case, smaller generators were used so that relatively large values of x/h or x/θ could be achieved within the length of the wind tunnel working section, thus allowing for approximate self-preservation to be attained. Since different values of h were used for the near-wake and far-wake measurements, the corresponding blockages were also different (a constant blockage ratio of 3.6% applied to the near-wake measurements; smaller ratios, with a minimum of 0.8%, applied to the far-wake data). For the near-wake data, the Reynolds number Re ($\equiv U_\infty h/\nu$) was constant ($= 5600$) although $Re_\theta \equiv U_\infty \theta/\nu$ varied in the range 1800–4700. The far-wake data were obtained for different values of Re_h and Re_θ , as shown in Table 1.

Ideally, all measurements should have been carried out for the same blockage ratio and Reynolds number. For the reasons given above, this would have been very difficult to achieve. Nevertheless, the near-wake comparison (same blockage and Re_h) should be valid. Comparison in the far-wake for different generators should also be satisfactory since the attainment of approximate self-preservation is unlikely to depend strongly on the Reynolds number, provided it is sufficiently large.

Orthogonal arrays of sixteen X-wire probes were used for the simultaneous measurement of velocity fluctuations u, v in the (x, y) plane and u, w in the (x, z) plane. The arrays were attached to separate traversing mechanisms and could be moved independently of each other. The eight X-wires in the (x, y) plane were fixed with the second X-wire (from the bottom) positioned on the centreline; the eight X-wires in the (x, z) plane could be displaced in the y direction. The physical blockage caused by these arrays, cables and supports was estimated to be about 3%. Several types of measurements (Zhou and Antonia 1994) indicated that the interference to the flow due to the two arrays was negligible.

Wollaston (Pt-10% Rh) wires, 5 μ m in diameter and about 1 mm in working length, were operated with constant temperature circuits. Signals from the circuits were offset, amplified and then digitised using two 16 channel (12 bit) A/D boards and two personal computers (NEC 386) at a sampling

frequency of 3.5 kHz per channel. Data acquisition by the two computers was synchronised using a common external trigger pulse (the configuration has been shown by Krogstad et al. 1992). Using velocity and yaw calibrations, signals proportional to u , v and w , together with the local mean velocities, \bar{U} , \bar{V} (≈ 0) and \bar{W} (≈ 0), were formed on digital tape. The duration of each record was about 38 s. Subsequent data processing was done on a VAX 8550 computer.

3 Mean velocity, Reynolds stresses and v spectra

Distributions of $1 - (U_\infty^* - \bar{U}^*)$, $\overline{u^{*2}}$, $\overline{v^{*2}}$ and $\overline{u^*v^*}$ are shown in Fig. 2. An asterisk denotes normalisation by the maximum velocity defect U_1 and/or the half-width L (see Fig. 1). For each generator, the profiles are shown at two x locations, sufficiently far apart, the upstream one being large enough to be considered in the far-wake. The profiles show reasonable collapse, indicating that self-preservation is approximately attained. Note that the difference $(U_\infty^* - \bar{U}^*)$ is 1 on the centreline and zero in the freestream. The collapse of distributions for $1 - (U_\infty^* - \bar{U}^*)$, the difference between the local mean velocity and the mean velocity on the centreline, is approximately independent of the wake generator. This is probably the result of using U_1 and L as the normalising scales. In the case $\overline{u^{*2}}$, $\overline{v^{*2}}$ and $\overline{u^*v^*}$, there are significant variations, which lie outside the estimated experimental uncertainty band

of about 10%, between distributions for different generators. Although $\overline{u^*v^*}$ has approximately the same shape when different generators are used, $\overline{u^{*2}}$ and $\overline{v^{*2}}$ exhibit different shapes. The difference is particularly noticeable between the square cylinder wake and the other flows. While the possibility that the variations may disappear at infinitely large values of x/θ cannot be ruled out, the evidence in Fig. 2 points to initial conditions having a significant influence on the far-wake type of self-preservation that is achieved for values of x/θ typical of laboratory investigations.

The v spectrum is a relatively sensitive indicator of the presence of the organised (vortical) structures. Spectra of v are shown in Fig. 3 for both the near-wake (Fig. 3a) and far-wake (Fig. 3b). The product fF has been plotted versus the normalised frequency f^* ($\equiv fL/U_1$), where F is the spectral density defined such that $\int_0^\infty Fdf = 1$. A log-linear scale has been used in order to identify the frequencies which contribute most to the energy. The solid body near-wake distributions (Fig. 3a) exhibit sharp peaks; when normalised by h and U_∞ , the magnitude of this peak frequency is identical (≈ 0.21) for the circular and triangular cylinders but smaller (≈ 0.13) for the square cylinder. The latter value is in reasonable agreement with both measurement (e.g. Vickery 1966; Durao et al. 1988; Lyn and Rodi 1994) and calculations (Franke and Rodi 1993). For the screen, the peak is smaller in amplitude and more widely spread apparently reflecting the absence of a primary

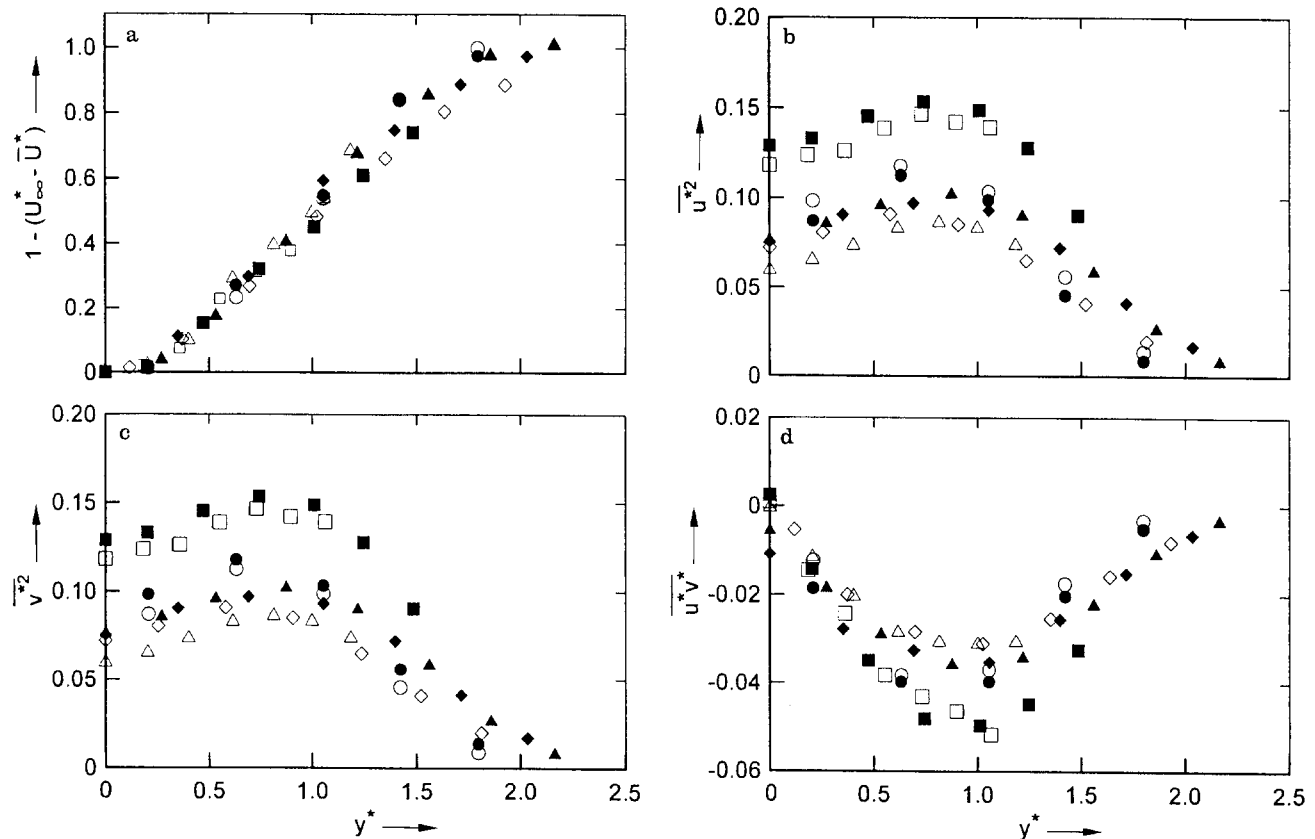


Fig. 2a-d. Lateral distributions of the mean velocity relative to the centreline velocity and of the Reynolds stresses. Circular cylinder: \bullet , $x/\theta = 780$; \circ , $x/\theta = 570$. Triangular cylinder: \blacktriangle , 240; \triangle , 550. Square cylinder: \blacksquare , 180; \square , 410. Screen: \blacklozenge , 300; \diamond , 830. a $1 - (U_\infty^* - \bar{U}^*)$; b $\overline{u^{*2}}$; c $\overline{v^{*2}}$; d $\overline{u^*v^*}$.

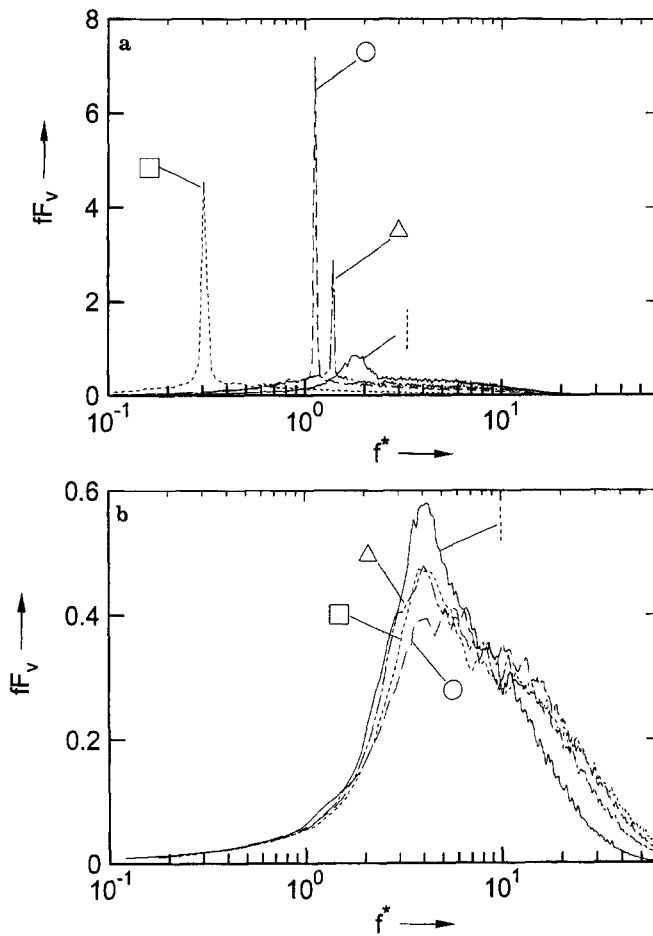


Fig. 3a, b. Spectra of v . a near-wake; b far-wake ($y^* \approx 1$)

vortex street in this flow. There is significantly more high frequency energy in this flow than in the solid body wakes; this difference may suggest a slower evolution to a self-preserving state for the solid body wakes. The spectra in the far-wake (Fig. 3b) are closer together, the location of the peak frequency being approximately the same for all generators, apparently consistent with the expectation that large structures should scale with L (Antonia et al. 1987). Note however that the magnitude of the peak energy varies among different generators. This variation cannot be ignored since it is larger than the experimental uncertainty which would apply to any particular curve; Fig. 4 shows that the v spectra ($y^* \approx 1$) at two different x locations in the triangular cylinder wake are in close agreement with each other, in conformity with the suggestion that a state of local self-preservation has been achieved in that flow. The differences in the high frequency part of the spectra in Fig. 3b are expected since the appropriate normalising scales in this region should be the Kolmogorov velocity scale and Kolmogorov length scale.

Bevilaqua and Lykoudis (1978) observed a difference in the self-preserving state between the wakes of a sphere and a porous disk, and proposed that this difference was due to a difference in the mechanism responsible for self-preservation. For the porous disk, it was conjectured that vortical structures resulted from the straining of the turbulence by the mean flow, the flow development being controlled by

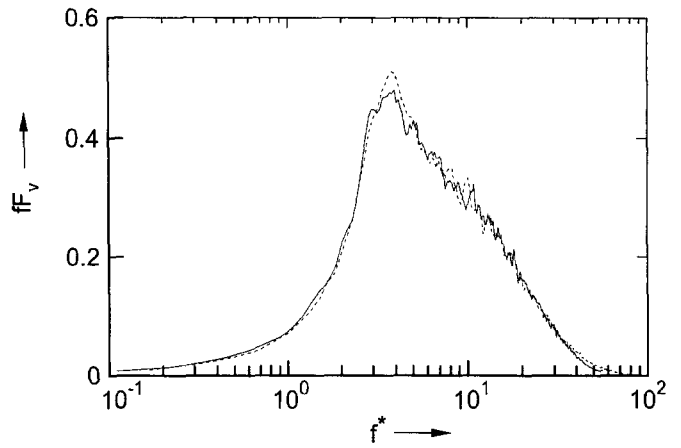


Fig. 4. Spectra (smoothed) of the lateral velocity fluctuation v at $y^* \approx 1$ in the wake of the triangular cylinder. —, $x/\theta = 240$; ---, 550

a vortex stretching mechanism. For the sphere, it was suggested, on the basis of flow visualisations, that vortical structures shed from the sphere persisted well downstream and the flow development was controlled by this persistence. Flow visualisation may, however, be misleading if flow markers are not released locally (Hussain 1986; Cimbalá et al. 1988). Cimbalá et al. confirmed that far-wake structures did not depend directly on the scale of frequency of the primary vortex street in the near-wake, thus refuting the conjecture (e.g. Matsui and Okude 1983; Bevilaqua and Lykoudis 1978) that they resulted from the persistence or amalgamation of the primary vortices. Browne et al. (1989) measured a non-zero correlation between v fluctuations obtained with a fixed X -probe at $x/h = 200$ and a moving X -probe displaced in the range $0 < x/h < 200$ in a circular cylinder wake. They suggested that the far-wake structures might originate in the near-wake, perhaps immediately downstream of the cylinder (although this does not necessarily imply a connection between the far-wake structures and the primary vortex street). If this scenario is true, it is not surprising that initial conditions may have an effect on vortical structures in the self-preserving region.

4 RMS vorticity

Although vorticity measurements have been reported in both near- and far-fields of a circular cylinder, the effect of initial conditions on vorticity has not been considered. The instantaneous lateral and spanwise components of vorticity were approximated as follows

$$\left. \begin{aligned} \omega_y &\approx \frac{\Delta U}{\Delta z} - \frac{\Delta W}{\Delta x} \\ \omega_z &\approx \frac{\Delta V}{\Delta x} - \frac{\Delta U}{\Delta y} \end{aligned} \right\} \quad (1)$$

where $U = \bar{U} + u$, $V = v$ and $W = w$. Δy or Δz (≈ 5 mm) is the spacing between X -wires and $\Delta x \approx -\Delta t \bar{U}$ ($= 1.4 \sim 1.8$ mm), where Δt is the time interval. In the computation of vorticity, the central difference approximation (e.g. Hussain and Hayakawa 1987) was used so that the array of eight X -wires in

each plane gave the instantaneous vorticity at each of the seven midpoints between adjacent X-wires. The relatively large spacing between X-wires degraded the spatial resolution of vorticity. (For the circular cylinder wake, the Kolmogorov length is about 0.3 mm at $x/\theta \approx 580$ and $Re_\theta = 1300$). This is not critical in the context of comparing the rms vorticity among different flows since the degradation should be about the same in each flow.

The distribution of $\omega_z'^*$ is shown in Fig. 5, where the prime denotes a rms quantity. It appears that for the same downstream position, $\omega_z'^*$ decreases as y^* increases. For solid body wakes, the value of $\omega_z'^*$ is considerably larger in the

near-field than in the far-field. The decrease (about 40% at $y^* = 0.5$) reflects mainly the decay of the primary vortex street. For the screen wake, however, $\omega_z'^*$ increases (also by about 40%) between the near-field and the far-field, consistent with the absence of a primary vortex street in this flow. While accurate one-point vorticity data at a greater number of x stations would be desirable, the present results indicate that the streamwise evolution of the vortical field is significantly different for the screen wake than for the solid body wakes. There is a large spread in $\omega_z'^*$ in the near-field for different wake generators. While this spread reduces in the self-preserving region, it does not disappear. In both near- and far-fields, $\omega_z'^*$ is largest for the square cylinder wake and smallest for the screen wake, whereas it is nearly the same for the circular and triangular cylinders.

Marasli et al. (1993) and Antonia et al. (1988), found that $\omega_y'^*$ does not vary greatly with y/L when $y/L \leq 1$. Therefore, $\omega_y'^*$ was estimated at $y^* \approx 0.5$. The magnitude of $\omega_y'^*$ is comparable to $\omega_z'^*$ and differs among wakes. For the solid body wakes, $\omega_y'^*$, like $\omega_z'^*$, decreases (by about 40%) between the near-field and the far-field. In the screen wake, there is an increase of about 30%, comparable to the increase observed in $\omega_z'^*$.

5 Structural characteristics

Vortical structures were detected using the iterative spanwise vorticity-based method described by Zhou and Antonia (1993). The final detections, obtained along the average vortex path, were used to obtain conditional sectional streamlines and contours of the coherent components of the Reynolds stresses. Conditional sectional streamlines shown in Fig. 6, were

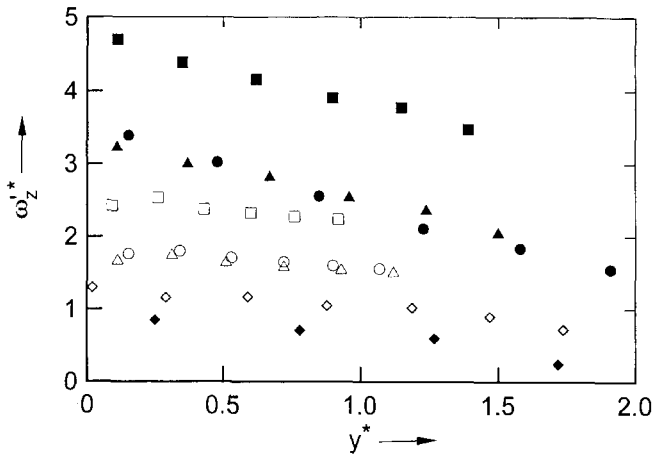


Fig. 5. Root mean square spanwise vorticity. Circular cylinder: ●, $x/\theta = 42$; ○, $x/\theta = 580$. Triangular cylinder: ▲, 33; △, 550. Square cylinder: ■, 24; □, 410. Screen: ◆, 61; ◇, 830

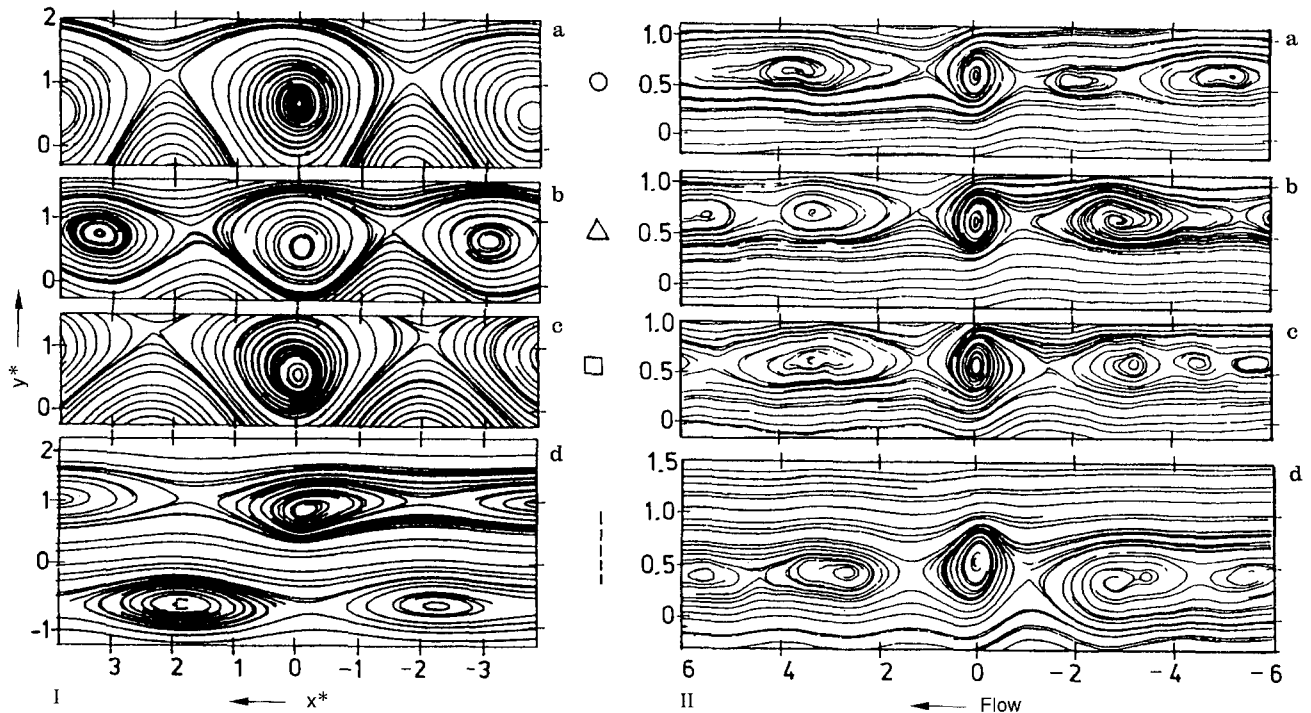


Fig. 6a-d. Conditional sectional streamlines in the (x^*, y^*) plane. (i) near-wake; (ii) far-wake. a circular cylinder; b triangular; c square; d screen

calculated (by a method described in Bisset et al. 1990) in a frame of reference translating with a velocity equal to U_c . For convenience, the space-time transformation $x \equiv -tU_c$ has been used to display the results in the (x, y) plane. The origin $x=0$ corresponds to the detection instant. In both near and far-wakes, U_c was determined to be the mean velocity at the location of maximum spanwise vorticity. Several other methods were used in the near-wake, all yielding essentially the same numerical values for U_c (see Zhou and Antonia 1992, for details).

The near-wake patterns [Fig. 6(i)] exhibit large variations in periodicity, shape and size; although Kármán-like patterns are also identifiable in the screen wake, Fig. 6(i) d, they differ from those for the solid body wakes. Near the detection instant, the patterns in the screen wake are asymmetrical, a behaviour exhibited by all the far-wake patterns in Fig. 6(ii).

The near-wake (x, z) plane sectional streamlines (Fig. 7(i) a, b, c) near the detection instant are generally aligned with the x direction in the solid body wakes, indicating a negligible lateral vorticity. The corresponding streamlines in the screen wake (Fig. 7(i) d) exhibit counter-rotating patterns, reminiscent of the double roller patterns of the far-wake of a circular cylinder (e.g. Grant 1958; Mumford 1983; Ferré et al. 1990). Comparison between Fig. 7(i) d and Fig. 7(ii) suggests a similarity between structures in the screen near-wake and those in the far-wake, where counter-rotating patterns are observed for each generator.

The coherent contribution to the Reynolds stresses may be measured through the ratio $\overline{\tilde{\beta}\tilde{\gamma}}/\overline{\beta\gamma}$ as defined in Zhou and Antonia (1994). Here β, γ each stand for either u or v ; the tilde refers to the coherent component and the double overbar denotes averaging over the mean period between structures.

The maximum values of $\overline{\tilde{\beta}\tilde{\gamma}}/\overline{\beta\gamma}$ occur at the vortex centre location and are shown in Table 2. For the solid body far-wakes, the magnitude is quite different from that in the near-wakes. The maximum values of $\overline{\tilde{u}^2}/\overline{u^2}$ and $\overline{\tilde{v}^2}/\overline{v^2}$ in the near-wakes are in the range 30–50%, larger than those (20–25%) in the far-wakes. But the maximum value of $\overline{\tilde{u}\tilde{v}}/\overline{uv}$ in the near-wake appears smaller, not exceeding 20%, than that (25–30%) in the far-wake. The difference in the coherent contribution to \overline{uv} between the solid body near- and far-wakes is consistent with the differences observed in the contours of $\tilde{u}\tilde{v}$ (Fig. 8). These contours exhibit a clover-leaf pattern (as noted by Hussain and Hayakawa 1987) in each case. In the solid body near-wakes (Fig. 8(i) a–c), the contours are reasonably symmetrical with respect to x about the vortex centres. This symmetry implies a small contribution to \overline{uv} since this contribution is determined by the balance between positive and negative $\tilde{u}\tilde{v}$ within the structures. In the solid body far-wakes, the size and levels of the $\tilde{u}\tilde{v}$ contours (Fig. 8(ii) a–c) are larger in the first ($\tilde{u} > 0, \tilde{v} > 0$) and third ($\tilde{u} < 0, \tilde{v} < 0$) quadrants than in the other two quadrants. This

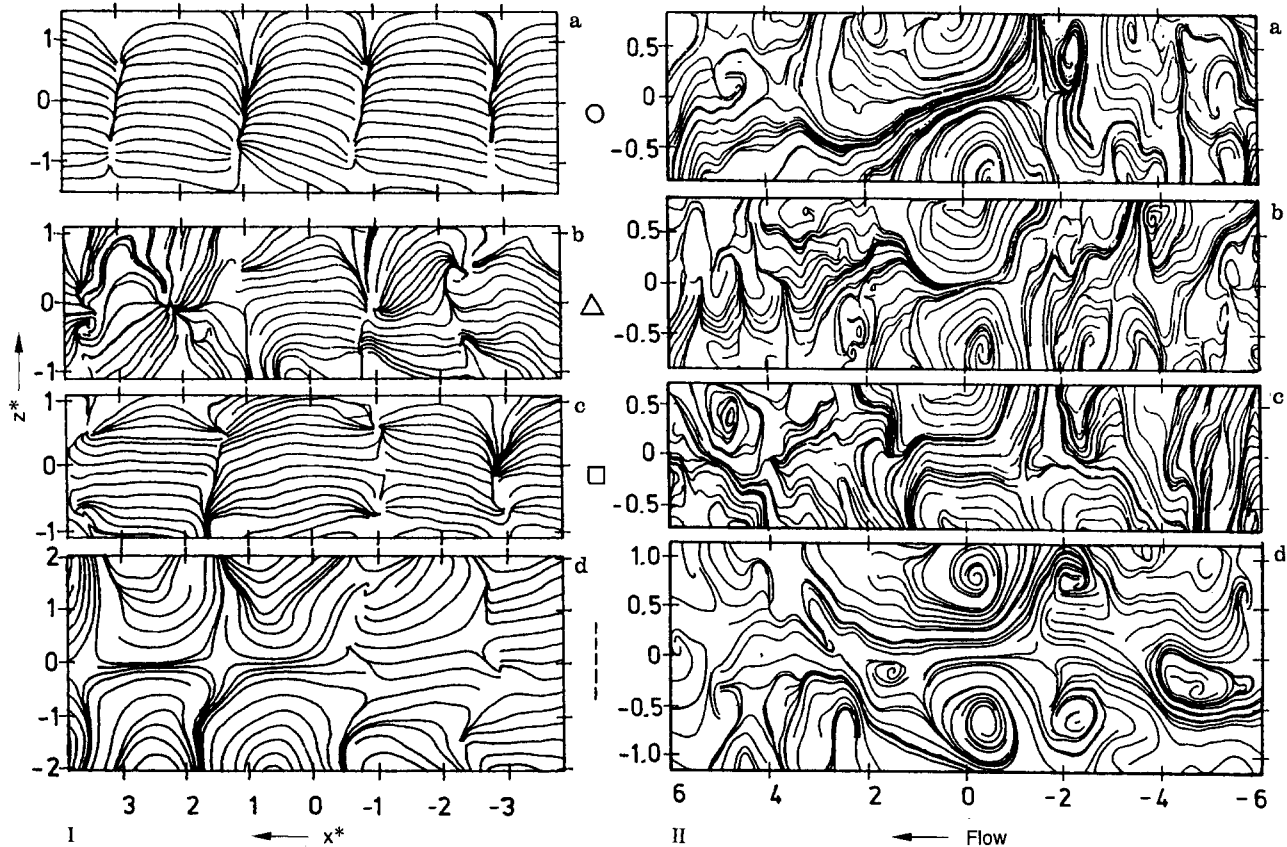


Fig. 7a–d. Conditional sectional streamlines in the (x^*, z^*) plane. (i) near-wake; (ii) far-wake. a circular cylinder; b triangular; c square; d screen

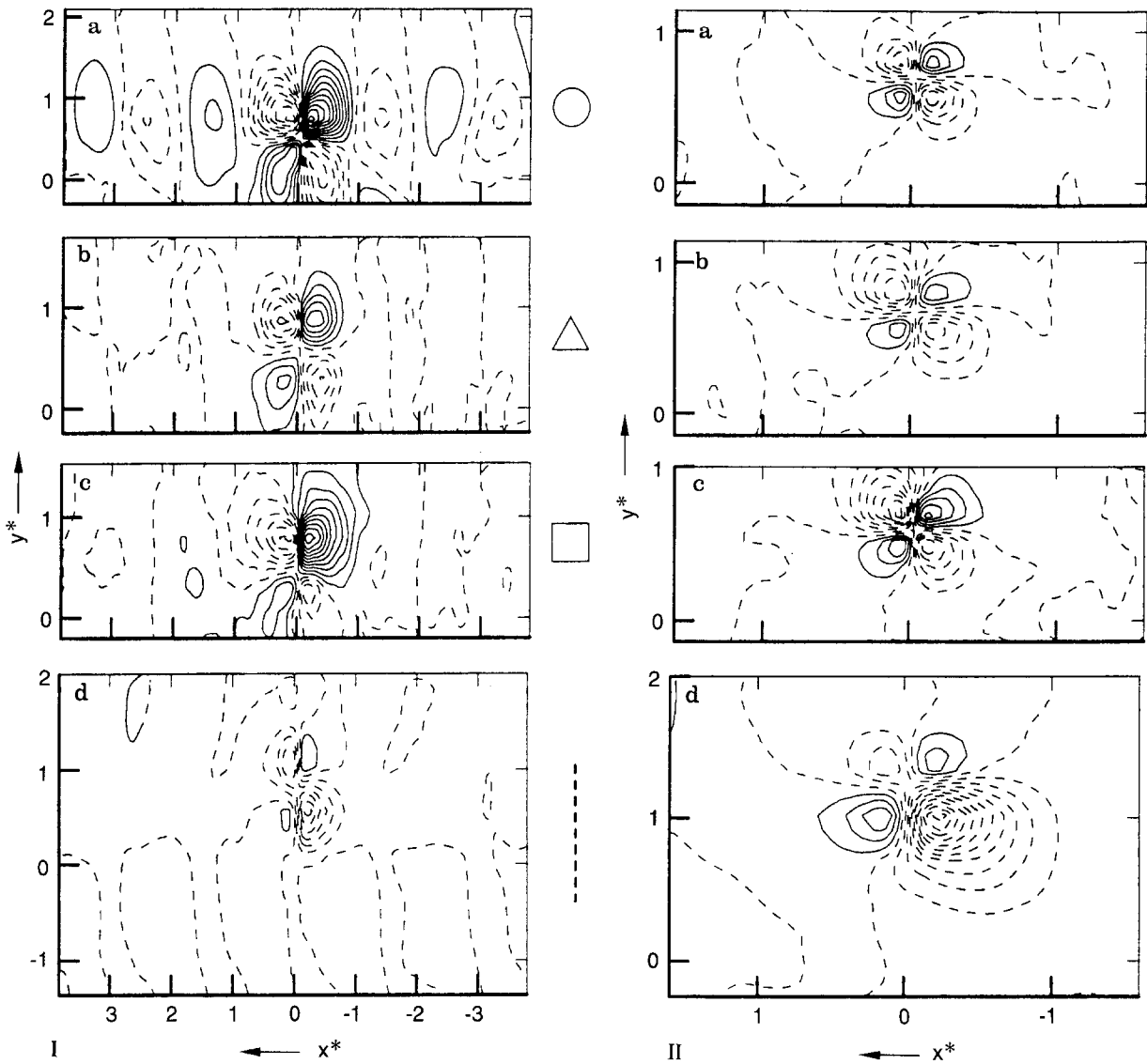


Fig. 8a-d. Contours of $\tilde{u}^*\delta^*$ in the (x^*, y^*) plane. (i) near-wake: **a** circular cylinder (contour levels = -0.4 to 0.6 , increment = 0.05 , $x/\theta = 42$); **b** triangular (-0.15 to 0.15 , 0.05 , 33); **c** square (-0.3 to 0.45 , 0.05 , 24); **d** screen (-0.03 to 0.005 , 0.005 , 61). (ii) far-wake: **a** circular cylinder (contour levels = -0.05 to 0.03 , increment = 0.01 , $x/\theta = 580$); **b** triangular (-0.05 to 0.02 , 0.01 , 550); **c** square (-0.08 to 0.05 , 0.01 , 410); **d** screen (-0.11 to 0.03 , 0.01 , 830)

asymmetry will result in a relatively large contribution to \overline{uv} . Speculatively, this asymmetry results from the interaction between the structures and the shear. Since the near-wake structures are strongly rotational (the vorticity is large and the phase between u and v is about -90°) they may not be significantly affected by the shear. On the other hand, the far-wake structures are weak (the vorticity is small and the phase between u and v is nearly 180°) and more likely to be influenced by the shear.

For the screen near-wake, the maximum values of $\overline{\tilde{u}^2}/\overline{u^2}$ and $\overline{\tilde{v}^2}/\overline{v^2}$ (Table 2) are comparable to those in the solid body near-wakes, but the maximum value of $\overline{\tilde{u}\tilde{v}}/\overline{uv}$ is over 40%, significantly larger than that in the solid body near-wakes. Structures in the screen wake do not appear to be strongly rotational; their peak vorticity is much smaller than that in the solid body wakes. Also, the phase shift between u and v is close

to 180° and the influence of the shear is more likely to be important. The $\tilde{u}\tilde{v}$ contours (Fig. 8(i)d and 8(ii)d) are strongly asymmetrical with respect to x (about the vortex centre), resulting in a relatively large contribution to \overline{uv} .

The maximum values (35–50%) of $\overline{\tilde{\beta}\tilde{\gamma}}/\overline{\beta\gamma}$ in the screen far-wake remain appreciably different from those (20–30%) in the solid body far-wakes. The structures in the screen wake have a relatively weak peak vorticity, by comparison to those in the solid body wakes, implying that the influence of the shear may be large. Correspondingly, the asymmetry of the $\tilde{u}\tilde{v}$ contours (Fig. 8(ii)) appears to be especially prominent in the screen wake. Therefore, the coherent contribution to \overline{uv} is appreciably larger in the screen far-wake than in the solid body far-wake. The difference further underlines the slow disentanglement from initial conditions.

Table 2. Maximum coherent contributions to the Reynolds stresses

Wake generator	x/θ	$\overline{\tilde{u}^2}/\overline{u^2}$ (%)	$\overline{\tilde{v}^2}/\overline{v^2}$ (%)	$\overline{\tilde{u}\tilde{v}}/\overline{uv}$ (%)
Circular cylinder	580	27	19	26
	42	34	44	4
Triangular cylinder	550	27	23	30
	33	28	44	21
Square cylinder	410	20	20	24
	24	28	55	18
Screen	830	46	35	49
	61	18	41	44

The screen near- and far-wake structures exhibit a close similarity, with virtually the same values (35–50%) for $\overline{\tilde{v}^2}/\overline{v^2}$ and $\overline{\tilde{u}\tilde{v}}/\overline{uv}$. There is a correspondingly close similarity between the $\tilde{u}\tilde{v}$ contours of Fig. 8(i)d and those in Fig. 8(ii)d; it would appear that the structures in this flow are more likely to survive than those in the solid bodies.

6 Conclusion

Turbulent plane wakes of various wake generating bodies have been investigated experimentally, primarily to ascertain whether differences can be discerned in the far-wake and whether they are related to differences in the near-wake. For each wake, approximate self-preservation appears to be supported by the data. However, Reynolds stresses, spectra and rms vorticity distributions in the self-preserving region are not universal; they differ for different wake generators. This points to a persistence of the initial conditions, consistent with various experimental observations (e.g. Wygnanski et al. 1987) and the analysis of George (1989).

The non-universality of the self-preserving distributions reflects the dependence of the large-scale structures on the wake generator. The rms vorticity components in the solid body wakes are relatively large by comparison to the screen wake. A possible explanation for this is that the far-wake structures reflect to a large extent the properties of the secondary vortex street which forms in the near-wake. For the solid body wakes, these secondary structures are influenced, for example, through stretching, by the primary vortices that are shed from the body surface. This influence may in turn strengthen the secondary structures, resulting in a relatively large rms vorticity in the self-preserving region. Conditional sectional streamlines and contours of $\tilde{u}\tilde{v}$ indicate that the vortical structures in the self-preserving screen wake are more asymmetrical than in the self-preserving solid body wakes. Accordingly, the contribution to the Reynolds shear stresses is appreciably larger in the screen wake than in the solid body wakes.

The close similarity between the near-field structures and those in the far-field in the screen wake indicates that the structure formation mechanism may be the same throughout this flow. While the possibility of decay and regeneration of the structures is not excluded, it is conjectured that, once formed, they may survive a long distance. Browne et al. (1989) observed

a broad peak in the v spectrum as well as a narrow spike at the shedding frequency in the near-wake of a circular cylinder. This indicated the existence of structures with different scales and spacings in this flow region. They suggested that closely spaced structures, mainly the primary vortices, were likely to be destroyed due to strong interaction with each other, while the more widely spaced secondary structures could survive for long distances. They proposed that the far-wake structures had their origin in the near-wake, perhaps immediately downstream of the cylinder. This proposition is consistent with the speculation that horseshoe-like vortex structures can form at the cylinder. Note that the vorticity of the screen near-wake structures is weaker than that of the primary structures in the solid body near-wakes. It can be surmised that there is only weak interaction between structures in the screen wake; this is supported by the conditional sectional streamlines in Fig. 6(i)d. One would expect these structures to have a high survival rate.

The solid body far-wake structures appear to bear little resemblance to the near-wake primary structures (the secondary structures are relatively weak and are consequently undetected by the present scheme). The dynamical process for the formation of far-wake structures in these flows appears to be more complicated than in the screen wake. It is likely, for example, that, following the break up of the primary vortices, smaller eddies are formed (Giralt and Ferré 1993). This would tend to delay the establishment of the far-wake structures and retard the onset of self-preservation. Data collected in the course of the present experiments suggest that self-preservation of the Reynolds stresses is attained more rapidly in the case of the screen; a more detailed investigation is however required to confirm this suggestion.

References

- Antonia RA; Browne LWB; Fulachier L (1987) Average wavelength of organised structures in the turbulent far wake of a cylinder. Expts in Fluids 5: 298–304
- Antonia RA; Browne LWB; Shah DA (1988) Characteristics of vorticity fluctuations in a turbulent wake. J Fluid Mech 189: 349–365
- Bevilaqua PM; Lykoudis PS (1978) Turbulence memory in self-preserving wakes. J Fluid Mech 80: 589–606
- Bisset DK; Antonia RA; Browne LWB (1990) Spatial organization of large structures in the turbulent far wake of a cylinder. J Fluid Mech 218: 439–461
- Bonnet J-P; Delville J; Garem H (1986) Space and space-time longitudinal velocity correlations in the turbulent far wake of a flat plate in incompressible flow. Expts in Fluids 4: 189–196
- Browne LWB; Antonia RA; Shah DA (1989) On the origin of the organised motion in the turbulent far-wake of a cylinder. Expts in Fluids 7: 475–480
- Cimbala JM; Nagib HM; Roshko A (1988) Large structure in the far wakes of two-dimensional bluff bodies. J Fluid Mech 190: 265–298
- Durao DFG; Heitor MV; Perreira JCF (1988) Measurements of turbulent and periodic flows around a square cross-section cylinder. Expts in Fluids 6: 298–304
- Franke R; Rodi W (1993) Calculation of vortex shedding past a square cylinder with various turbulence models, in F Durst, R Friedrich, BE Launder, FW Schmidt, U Schumann and JH Whitelaw (eds.) Turbulent Shear Flows 8, Springer: 189–204
- George WK (1989) The self-preservation of turbulent flows and its relation to initial conditions and coherent structures, in WK George and R Arndt (eds.) Advances in Turbulence, Berlin, Springer: 39–74
- Giralt F; Ferré JA (1993) Structure and flow patterns in turbulent wake. Phys Fluids A 5: 1783–1789

- Hussain AKMF** (1986) Coherent structure and turbulence. *J Fluid Mech* 173: 303–356
- Hussain AKMF; Hayakawa M** (1987) Eduction of large-scale organized structures in a turbulent plane wake. *J Fluid Mech* 180: 193–229
- Kiya M; Matsumura M** (1985a) Large-scale and small-scale turbulence structures in the intermediate wake of a two-dimensional normal plate. *Bulletin of JSME* 28: 1054–1061
- Kiya M; Matsumura M** (1985b) Turbulence structure in intermediate wake of a circular cylinder. *Bulletin of JSME* 28: 2617–2624
- Krogstad P-Å; Antonia RA; Browne LWB** (1992) Structure investigation in a turbulent boundary layer using orthogonal X-wire arrays, in MR Davis and GJ Walker (eds.) *Proc Eleventh Australian Fluid Mechanics Conference Hobart*: 251–254
- Louchez PR; Kawall JG; Keffer JF** (1987) Detailed spread on characteristics of plane turbulent wakes. *Proc 5th Symposium on Turbulent Shear Flows, Lecture Notes in Physics Springer*: 98–109
- Lyn DA; Rodi W** (1994) The flapping shear layer formed by flow separation from the forward corner of a square cylinder. *J Fluid Mech* 267: 353–376
- Marasli B; Nguyen P; Wallace JM** (1993) A calibration technique for multiple-sensor hot-wire probes and its application to vorticity measurements in the wake of a circular cylinder. *Expts in Fluids* 15: 209–218
- Matsui T; Okude M** (1983) Formation of the secondary vortex street in the wake of a circular cylinder, in R Dumas and L Fulachier (eds.) *Structure of Complex Turbulent Shear Flow, Berlin, Springer*: 156–164
- Matsumura M; Huang Z; Kawall JG; Keffer JF** (1991) Coherent structures in the turbulent wake of a porous body. *Proc Eighth Symposium on Turbulent Shear Flows Munich*: 28-2
- Vickery BJ** (1966) Fluctuating lift and drag on a long cylinder of square cross-section in a smooth and turbulent stream. *J Fluid Mech* 25: 481–494
- Wynanski I; Champagne F; Marasli B** (1986) On the large-scale structures in two-dimensional, small-deficit, turbulent wakes. *J Fluid Mech* 168: 31–71
- Zhou Y; Antonia RA** (1992) Convection velocity measurements in a cylinder wake. *Expts in Fluids* 13: 63–70
- Zhou Y; Antonia RA** (1993) A study of turbulent vortices in the near-wake of a cylinder. *J Fluid Mech* 253: 643–661
- Zhou Y; Antonia RA** (1994) Critical points in a turbulent near-wake. *J Fluid Mech* 275: 59–81